W. -T. Hsu, J. R. Clark, and C. T. -C. Nguyen, "A resonant temperature sensor based on electrical spring softening," *Digest of Technical Papers*, the 11th Int. Conf. on Solid-State Sensors & Actuators (Transducers'01), Munich, Germany, June 10-14, 2001, pp. 1484-1487.

# A Resonant Temperature Sensor Based on Electrical Spring Softening

Wan-Thai Hsu, John R. Clark, and Clark T.-C. Nguyen
Center for Wireless Integrated Microsystems
Department of Electrical Engineering and Computer Science
University of Michigan, Ann Arbor, MI 48109-2122, U.S.A.

## ABSTRACT

A high-resolution resonant temperature sensor based on resonance frequency shifts caused by thermally-induced changes in the electrical spring stiffness across the capacitive transducer of a 10.7 MHz μmechanical resonator has been demonstrated with a sensitivity as high as −347ppm/°C (or −3.7kHz/°C). This sensor exhibits a fairly linear temperature-to-frequency transfer function with a slope (i.e., sensitivity) that can be controlled in real-time via adjustment of a dc-bias voltage $V_P$ applied to the resonator structure. Such adaptability makes this temperature sensor useful for applications requiring wide dynamic range.

**Keywords:** temperature, resonator, electrical stiffness.

## I. INTRODUCTION

Recent demonstrations of vibrating micromechanical ("μmechanical") resonators with frequencies up to mid-VHF and $Q$'s in excess of 3,000 [1] have spurred interest in the use of these devices as high-$Q$ tanks for bandpass filters and low-phase noise reference oscillators in communication transceivers and instrumentation [2]. Further incentive for doing this arises from the potential for single-chip integration of such devices alongside transistors, using a merged MEMS/transistor technology [3][4][5]. This ability to integrate RF MEMS devices with transistors might eventually facilitate the realization of switchable ultra-high-$Q$ filter banks for use in future RF channel-select transceiver architectures, expected to achieve substantial power savings (hence, battery lifetime) by trading power for $Q$ [2].

However, although the $Q$'s posted by vibrating μmechanical resonators have so far (up to low-UHF) been very encouraging for use in such channel-select architectures, there are still numerous hurdles to overcome before such a system can become a reality. Among the major obstacles is the finite thermal stability of μmechanical resonators, for which uncompensated frequency variations on the order of 1760 ppm over a 27°C to 107°C range are typical. Although passive compensation methods, such as geometric-stress compensation [6], have succeeded in lowering resonator temperature dependences down to ~200 ppm variation over a 27°C to 107°C range, this is still well short of the 1 ppm needed for a channel-select application.

To further improve thermal stability, electronic temperature compensation is desirable, in which intelligent feedback circuitry together with a precise temperature sensor are utilized to counteract temperature-induced frequency shifts [7]. From previous compensation work done for quartz crystal oscillators, the compensation circuit can be made most effective if the temperature sensor data governing the compensation can be derived from the resonator itself [8], or from a replica.

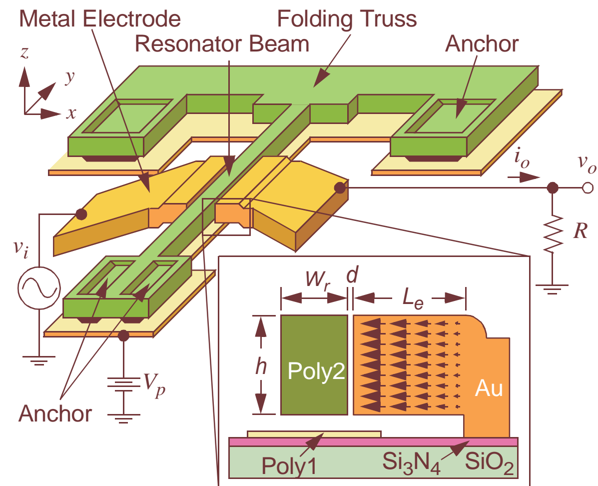


*Fig. 1: Perspective and cross-section views of an electrical-spring softening-based resonant temperature sensor.*

This paper describes a temperature sensor that satisfies this criterion, in which resonance frequency shifts caused by thermally-induced changes in the electrical spring stiffness across the capacitive transducer of a μmechanical resonator are used to sense temperature shifts. Using this approach, resonant temperature sensors have been demonstrated with sensitivities as high as −347ppm/°C (or −3.7kHz/°C), and with fairly linear temperature-to-frequency transfer characteristics that can be adjusted via adjustment of the dc voltage drop across the electrode-to-resonator capacitive gap.

## II. DEVICE OPERATION AND DESIGN

Figure 1 presents a perspective-view schematic and cross section of the resonant temperature sensor, identifying key features and specifying a two-port bias and excitation configuration. As shown, the sensor consists of a lateral flexual-mode beam μmechanical resonator, fixed to the substrate at one end and held at the other by a folded suspension, all constructed in a high-$Q$ material (e.g., polysilicon). The resonator beam is flanked by two electrodes constructed in a material with a large thermal expansion coefficient (e.g., Au) relative to that of the substrate. As shown in Fig. 1, the resonator beam can be driven into resonance vibration by applying a voltage across the electrode-to-resonator gap comprised of the

sum of a dc-bias voltage $V_P$ and an ac signal $v_i$ at the beam resonance frequency $f_o$, which then combine to generate a force at the frequency of $v_i$ proportional to the product $V_P v_i$.

The device senses temperature shifts as frequency shifts caused by temperature-induced expansions/contractions of the electrodes. In particular, if the electrode-to-resonator gaps are small enough, then a temperature-induced $x$-directed expansion of the electrodes would cause a sizable fractional change in the electrode-to-resonator gap spacing $d$, leading to a change in the electrical spring stiffness $k_e$, which varies inversely with $d^3$ and proportionally with $V_P^2$ [1][9]. This in turn leads to a change in resonance frequency governed by [1]

$$f_o \cong f_{nom}\left\{1 - \frac{1}{2}\frac{V_P^2 \varepsilon_o h W_e}{[d_o + (\alpha_{sub} - \alpha_e)L_e(T - T_o)]^3 k_m}\right\} \quad (1)$$

where $f_{nom}$ is the center frequency of the resonator beam at a nominal temperature $T_o$ and with $V_P$=0V, $k_m$ is the integrated mechanical spring stiffness of the resonator at its midpoint [1], $d_o$ is the electrode-to-resonator gap spacing at $T_o$, $W_e$ is the width of the electrode, $L_e$ is the length of the suspended portion of the electrode (that is free to expand), $\alpha_e$ and $\alpha_{sub}$ are the thermal expansion coefficients of the electrode and substrate materials, respectively, and all other dimensions are given in Fig. 1.

Differentiating (1) with respect to temperature, then dividing by $f_o$, the temperature coefficient of the resonance frequency for this device can be expressed as

$$TC_{fo} = \frac{1}{f_o}\frac{\partial f_o}{\partial T} = \frac{3}{2}\frac{V_P^2 \varepsilon_o h W_e L_e}{d_o^4 k_m}(\alpha_{sub} - \alpha_e), \quad (2)$$

from which sensitivity can be obtained by multiplying by temperature $T_o$. For the case of a 10.7MHz polysilicon resonator beam using Au electrodes ($\alpha_e$=13ppm/$^o$C) on a Si substrate ($\alpha_{sub}$=2.6ppm/$^o$C), with $k_m$=2,415N/m, $L_e$=3.5µm, $W_e$=18µm, $d_o$=600Å, and $h$=3µm, (2) predicts a temperature coefficient $TC_{fo}$ of −344ppm/$^o$C for $V_P$=18V, and −513 ppm/$^o$C for $V_P$=22V, due to thermal expansion of the electrodes alone.

Note that the use of a folded suspension in this design attempts to employ geometric-stress compensation [6] to reduce frequency shifts caused by Young's modulus variations with temperature, making (2) the principal governing equation for temperature sensitivity.

## III. FABRICATION

From (2), it is apparent that the ability to achieve a tiny metal-electrode-to-resonator gap spacing $d_o$ is key to achieving adequate sensitivity in this temperature sensor. For this reason, the lateral sub-µm gap process previously described in [10] constitutes a nearly ideal technology for construction of this device. Figure 2 presents the cross-section of this technology, achieved via a combination of polysilicon surface micromachining (for the resonator beam), metal electroplating (for the electrodes), and a sacrificial sidewall spacer technique that defines the tiny, lateral electrode-to-resonator gaps.

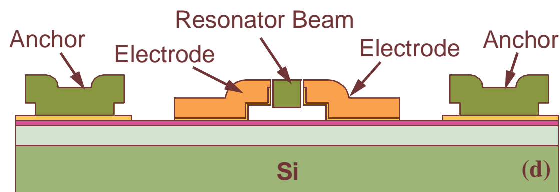


*Fig. 2: Cross-section of an electrical spring softening-based resonant temperature sensor achieved using a sacrificial sidewall spacer technology.*

**Table I: Resonant Temperature Sensor Design Summary**

| Parameter | Electrode Material | | Units |
|---|---|---|---|
| | Au | Poly-Si | |
| µBeam Dimens: $L_r/W_r/h$ | 40/2.45/3 | 40/2.2/3 | µm |
| Electrode Width, $W_e$ | 18 | 18 | µm |
| Electrode-to-Res.Gap, $d_o$ | 565 | 10,000 | Å |
| Free Electrode Length, $L_e$ | 3.5 | 4.5 | µm |
| DC-Bias Voltage, $V_P$ | 18 | 200 | V |
| Quality Factor, $Q$ | 5,000 | N/A | — |
| Motional Resistance, $R_x$ | 8.8 | 2,000 | kΩ |
| Pred. Temp. Coeff., $TC_{fo}$* | −344 | −16 [6] | ppm/$^o$C |
| Meas. Temp. Coeff., $TC_{fo}$* | −347 | −15 | ppm/$^o$C |
| Predicted Sensitivity, $S_T$* | 10.3 | 0.48 | % |
| Measured Sensitivity, $S_T$* | 10.4 | 0.45 | % |

* At $T$=300K.

## IV. EXPERIMENTAL RESULTS

To evaluate the performance of this temperature sensor, two variants of Fig. 1 were fabricated: (1) one with gold electrodes, expected to exhibit a strong temperature sensitivity; and (2) another with polysilicon electrodes, expected to be relatively stable with temperature, since the thermal expansion coefficients for polysilicon and the silicon substrate are nearly equal. This second variant is meant to serve as a reference designed to instill a greater appreciation for the degree of temperature sensitivity introduced by the expanding electrode concept described in Section II. Scanning-electron micrographs (SEM's) of each version are shown in Figs. 3(a) and 3(b), while Table I (together with Fig. 1) summarizes their specific geometric designs.

Measurements were made using a custom-built vacuum chamber featuring both dc and coaxial feedthroughs to external instrumentation, plus a port allowing insertion of an MMR Technologies temperature-controllable cantilever. For testing, resonator dies were mounted onto a pc board with a special interface to the MMR cantilever. Devices were directly bonded to pc board leads connected to board-mounted circuit elements in order to reduce parasitic feedthrough currents that could otherwise distort measured frequency characteristics. All

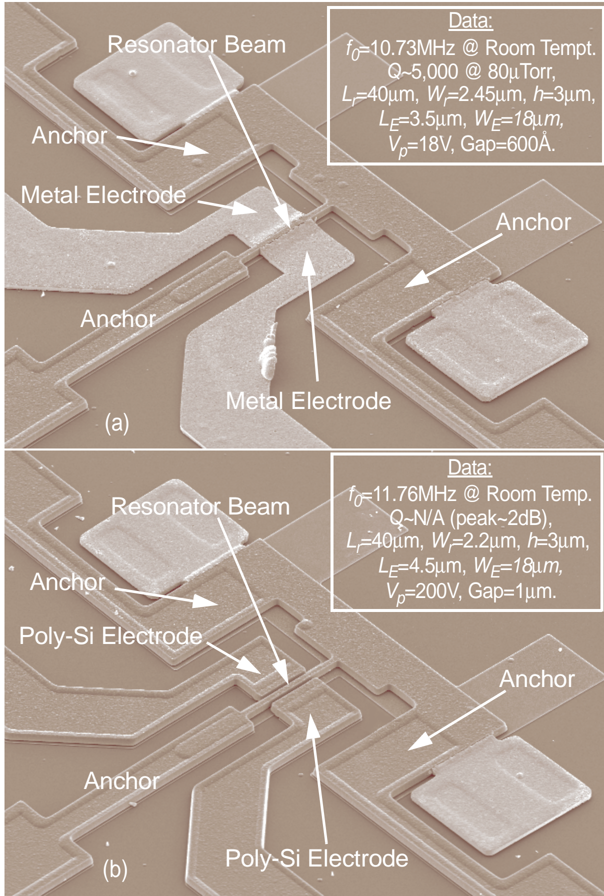


*Fig. 3: SEM photographs of fabricated resonant temperature sensors (a) with metal electrodes, (b) with polysilicon electrodes*

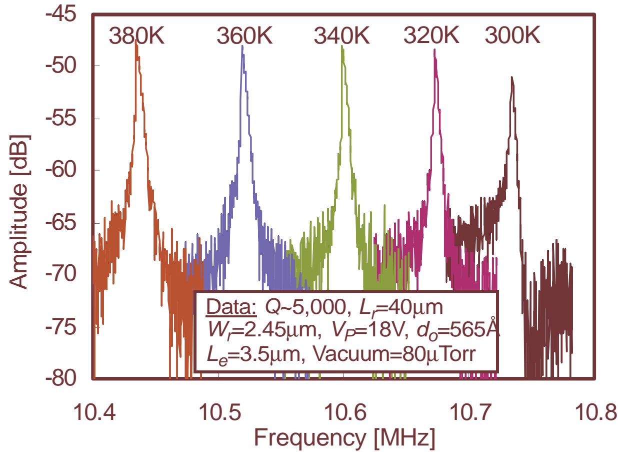


*Fig. 4: Measured frequency characteristics as a function of temperature for the device of Fig. 3(a).*

measurements were made under a pressure of 50 μTorr, provided by a turbo-molecular pump.

Measured frequency characteristics for the Au-electrode version of this device at various temperatures from 300K to 380K are shown in Fig. 4. The $Q$ of this resonator was around 5,000 for each temperature, which is somewhat larger than for comparable vertical-mode devices, possibly indicating smaller anchor losses in this lateral design. The increase in peak amplitude with increasing temperature observed in Fig. 4 serves as a first and direct indication that the electrode-to-resonator gap spacing shrinks as the temperature increases.

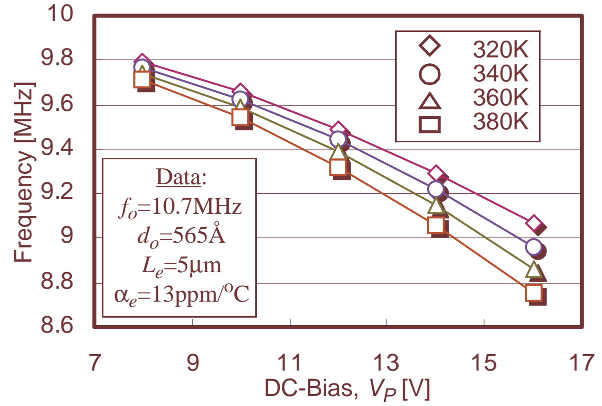


*Fig. 5: Measured resonance frequency versus dc-bias $V_P$ for the device of Fig. 3(a) at various temperatures.*

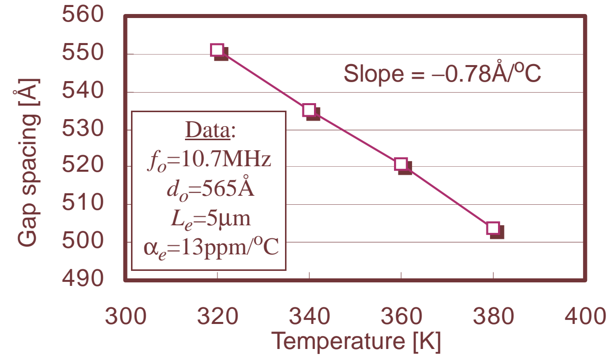


*Fig. 6: Electrode-to-resonator gap spacing $d_o$ versus temperature extracted from Fig. 5.*

To quantify the degree to which the electrode-to-resonator gap spacing $d_o$ changes as a function of temperature, an accurate method for determining $d_o$ is needed. As described in [1], in the absence of a means for direct visual determination (which is difficult given the tiny size of the gap), one very effective method for determining the electrode-to-resonator gap spacing involves first measuring and plotting the resonance frequency $f_o$ versus dc-bias $V_P$ for the μmechanical resonator in question, then fitting this curve to a more accurate form of (1), such as (12) in [1], using gap spacing $d_o$ as a fitting variable. Pursuant to determining gap spacing in this manner, Fig. 5 presents plots of $f_o$ versus $V_P$ for the resonator of Fig. 3(a) operated at various temperatures. Upon curve-fitting this data to (12) in [1], Fig. 6 presents a plot of electrode-to-resonator gap spacing versus temperature, showing a decreasing linear dependence of gap on temperature, changing at the rate of –0.78Å/°C—fairly close to the –0.65Å/°C expected from thermal expansion of the Au electrode alone.

Figure 7 presents measured curves of fractional fre-

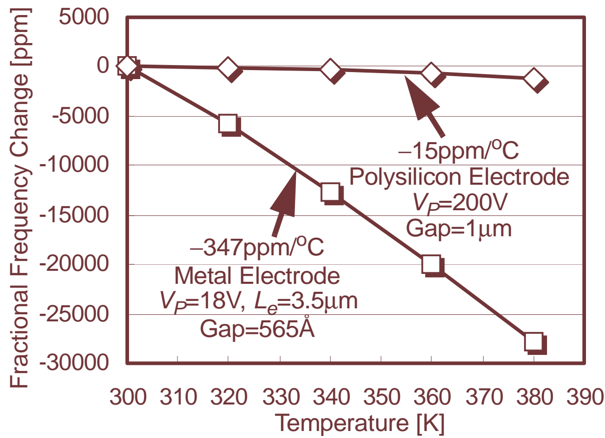


*Fig. 7: Fractional frequency change versus temperature for the metal-electrode and polysilicon-electrode resonant temperature sensors.*

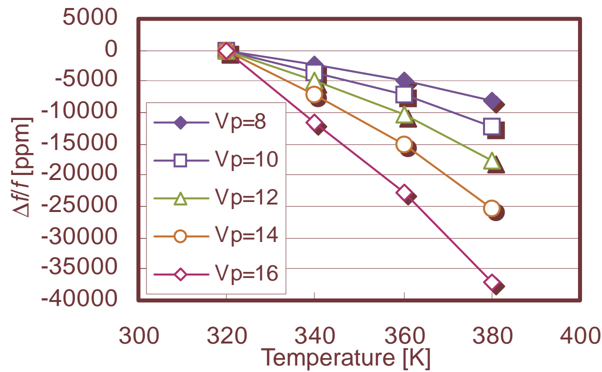


*Fig. 8: Measured plots of fractional frequency change versus temperature for the resonant temperature sensor of Fig. 3(a) at various values of dc-bias $V_P$.*

quency change versus temperature for each version of the resonant temperature sensor. For the polysilicon-electrode version, the $TC_{fo}$ of the resonance frequency, obtained from the slope of the $\Delta f/f$ curve, is only $-15$ ppm/°C (or 160 Hz/°C for $f_o$=10.7 MHz), which is consistent with previous numbers for vertically driven polysilicon resonator devices with polysilicon electrodes [11]. This small sensitivity is expected for this version, since the thermal expansion coefficient of the polysilicon electrodes is very close to that of the silicon substrate. This negates gap variation to first-order, and results in a $TC_{fo}$ governed mainly by the dependence of Young's modulus on temperature.

In sharp contrast, the thermal expansion coefficients for Au and Si are quite different, so the resonance frequency of the Au-electrode variant exhibits a much stronger dependence on temperature, on the order of $-347$ ppm/°C (or $-3.7$ kHz/°C)—a 23X increase over the polysilicon-electrode version that clearly demonstrates the range and utility of this sensor design. That the measured $TC_{fo}$ of the Au-electrode design is very close to the $-344$ppm/°C value predicted by (2) instills confidence in the formulations of Section II.

Figure 8 finally presents a measured plot of fractional

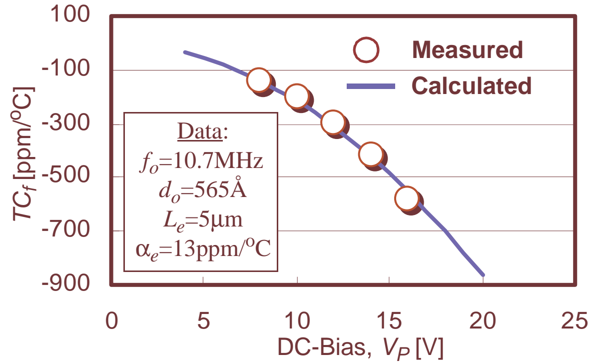


*Fig. 9: Measured and theoretical plots of temperature coefficient (obtained from Fig. 8) versus dc-bias $V_P$ for the Au-electrode T-sensor device of Fig. 3(a).*

frequency change $\Delta f/f$ versus temperature for the Au-electrode variant of the resonant temperature sensor for various values of dc-bias $V_P$. Using this data, Fig. 9 then plots measured temperature coefficients (i.e., sensitivities) as a function of $V_P$, along with the theoretical curve predicted by (2), showing an excellent fit between measurement and theory. The observed voltage-controllability, where a doubling of $V_P$ (from 8V to 16V) generates a 3.5X change in sensitivity, is quite strong, making this particular sensor very suitable for applications requiring wide dynamic range.

## V. CONCLUSIONS

A high-resolution resonant temperature sensor, based on electrical spring softening caused by thermal expansion of metal electrodes around a capacitively-driven µmechanical resonator, has been demonstrated with an eye towards application in temperature compensation circuitry for RF MEMS devices. The sensitivity of the device is controllable over a wide range via adjustment of a dc-bias voltage, and its resolution should be limited mainly by the phase noise floor of the closed-loop oscillator circuit used to sustain resonance oscillation. Efforts towards application of this sensor to temperature compensation are presently underway.

**Acknowledgment:** This work was supported under DARPA Cooperative Agmt. No. F30602-97-2-0101.

**References:**


[1] F.D.Bannon III, *et al.*, *IEEE JSSC,* v.35, No.4, pp.512-526, Apr.2000.

[2] C. T-C. Nguyen, *BCTM 2000*, pp. 142-149.

[3] T. A. Core, *et al.*, *Solid State Tech.*, pp. 39-47, Oct. 1993.

[4] A. E. Franke, *et al.*, *MEMS'99*, pp. 630-637.

[5] A.-C. Wong, *et al.*, *Transducers'01*, this digest.

[6] W.-T. Hsu, et al, IEDM'00, pp. 399-402.

[7] R. Achenbach, *et al.*, *IEEE JSSC*, v.35, No.10, pp.1502-1506, Oct.2000.

[8] S. Schodowski, *Symp. on Freq. Control*, 1989, pp.2-7.

[9] H. Nathanson, *et al.*, *IEEE Trans. Electron Devices*, vol. ED-14, no. 3, pp. 117-133, March 1967.

[10] W.-T. Hsu, et al, MEMS'01, pp 349-352.

[11] K. Wang, *et al.*, *IEEE/ASME JMEMS,* vol. 9, no. 3, pp. 347-360, Sept. 2000.